

## Analysis of the Inelastic Scattering of Alpha Particles. I

R. H. BASSEL AND G. R. SATCHLER

*Oak Ridge National Laboratory, Oak Ridge, Tennessee*

AND

R. M. DRISKO\* AND E. ROST\*†

*University of Pittsburgh, Pittsburgh, Pennsylvania*

(Received July 19, 1962)

The inelastic scattering of medium-energy alpha particles is interpreted as a direct interaction, using the distorted-waves theory. A deformed potential-well interaction based on the collective model of the nucleus is found to give results in good agreement with experiment. The parameters of the potential well are determined by fitting the elastic scattering, and the multipole deformations obtained from the magnitudes of the inelastic cross sections agree reasonably well with those obtained by other techniques. The effects on the theoretical predictions of variations in the parameters are described. Some preliminary study of the effects of including Coulomb excitation is also included.

### I. INTRODUCTION

THE inelastic scattering of medium-energy alpha particles provides perhaps the simplest and best understood examples of direct nuclear reactions.<sup>1</sup> Their analysis<sup>2</sup> has provided an insight into the behavior of other direct reactions, especially those involving particles which are strongly absorbed.<sup>3</sup>

The excitation of collective states is particularly amenable to study, firstly because these transitions are strongly enhanced and hence easily observed. Further, the over-all similarity of the initial and final nuclear states (which differ only in the degree of shape oscillation or rotation) leads one to suspect that the inelastic scattering to these states will bear a simple relationship to the elastic scattering. These ideas have been previously exploited in the adiabatic limit,<sup>4</sup> which assumes the energy loss in the inelastic transition is negligible, and treats the elastic and inelastic scattering on the same footing. In its simplest form this gives the well-known Fraunhofer diffraction model. Recently, more sophisticated developments in terms of partial waves have been given, which show even more clearly the relation between elastic and inelastic transitions in the adiabatic limit.<sup>5</sup>

The present paper is concerned with the distorted-waves (DW) method, which does not require the adiabatic assumption.<sup>1,2</sup> The so-called distorted-wave Born-

approximation amplitude [Eq. (1) below] contains the interaction responsible for the inelastic transition just once, so it describes a simple one-step process. The relative motion of the colliding pair before and after the inelastic event is described by distorted waves, which include the elastic scattering and are usually calculated using an optical-model potential. Then the transition is one between elastic scattering states, so the DW approximation assumes that elastic scattering is the dominant process and inelastic or reaction events can be treated as perturbations.

It has been shown<sup>2</sup> that the DW method is formally identical to the adiabatic method in the limit of weak coupling. It also has a number of advantages compared to other methods. It unifies the treatment of the inelastic scattering of strongly absorbed particles with that of nucleons (for which the adiabatic models are not so successful) and also with the treatment of other direct reactions such as stripping. The DW theory can use accurate elastic scattering wave functions (simply generated from appropriate optical potentials) whereas it is not so easy to incorporate these in the adiabatic methods. In particular, Coulomb effects are taken into account exactly. A further advantage is that of flexibility in allowing various parameters to be varied independently of any particular nuclear model, so that more physical phenomena can be explored.

DW calculations are impractical without the aid of a high-speed computer, although with access to such a machine they are very fast and not at all difficult to carry out. The simpler, approximate, models do not require computers, and generally give rise to fairly simple "universal" curves. While often giving a physical insight into various phenomena, they fit the experimental data in a qualitative way only (for example, giving peaks in the differential cross section at the correct angles). The two techniques are thus complementary to some extent.

The emphasis, in the present work, is on the use of the collective model (through the introduction of a nonspherical optical potential). Presumably the "correct"

\* Work partly performed while consultant at Oak Ridge National Laboratory.

† Present address: Palmer Physical Laboratory, Princeton University.

<sup>1</sup> N. Austern, in *Fast Neutron Physics, II*, edited by J. B. Marion and J. L. Fowler (Interscience Publishers, Inc., New York, 1962). This review contains many other references to this subject. See also R. M. Eisberg and C. E. Porter, *Revs. Modern Phys.* **33**, 190 (1961) for a discussion of elastic scattering.

<sup>2</sup> E. Rost and N. Austern, *Phys. Rev.* **120**, 1375 (1960).

<sup>3</sup> N. Austern, *Ann. Phys. (New York)* **15**, 299 (1961).

<sup>4</sup> J. S. Blair, *Phys. Rev.* **115**, 928 (1959); J. S. Blair and L. Wilets, *ibid.* **121**, 1493 (1961); S. I. Drozdov, *Soviet Phys.—JETP* **1**, 588, 591 (1955); **3**, 759 (1956); **7**, 889 (1958); **9**, 1335 (1959); E. V. Inopin, *ibid.* **4**, 764 (1957).

<sup>5</sup> J. S. Blair, D. Sharp, and L. Wilets, *Phys. Rev.* **125**, 1625 (1962); N. Austern and J. S. Blair (to be published).

interaction is a much more complicated object, but it is known that inelastic scattering (like electromagnetic transitions) is very sensitive to any collective correlations present in the nuclear wave functions.<sup>6</sup> Even if the initial and final states are well described (energetically) by the independent-particle model, some collective enhancement (such as due to coupling to core oscillations) is almost always present and often dominates over the "single-particle" contribution. Thus, the collective model picture is likely to have a wide range of validity.

Only the results of calculations for alpha particles are presented here, but the theory is applicable to other projectiles and the general results should be qualitatively true for other strongly absorbed particles, such as He<sup>3</sup>, with comparable energies.

## II. THE DISTORTED-WAVE THEORY

Consider the scattering of a particle with incident momentum  $\hbar\mathbf{k}_i$  and final momentum  $\hbar\mathbf{k}_f$ , in which the target nucleus is excited from a state  $v_i$  to a final state  $v_f$ . The distorted-wave theory is based upon a transition amplitude given by

$$T_{fi} = \int d\mathbf{r} \chi_{f^{(-)*}(\mathbf{k}_f, \mathbf{r})} \langle v_f | V | v_i \rangle \chi_{i^{(+)}}(\mathbf{k}_i, \mathbf{r}), \quad (1)$$

where the differential cross section is

$$(d\sigma/d\Omega) = (\mu/2\pi\hbar^2)^2 (k_f/k_i) \sum_{\text{av}} |T_{fi}|^2. \quad (2)$$

The  $\chi(\mathbf{k}, \mathbf{r})$  are the distorted waves which describe the *elastic* scattering of the particle by the nucleus before and after the inelastic transition. In the absence of a Coulomb field they have the asymptotic forms

$$\begin{aligned} \chi^{(+)}(\mathbf{k}, \mathbf{r}) &= \exp(i\mathbf{k} \cdot \mathbf{r}) + f(\theta) \exp(ikr)/r, \\ \chi^{(-)}(\mathbf{k}, \mathbf{r}) &= \exp(i\mathbf{k} \cdot \mathbf{r}) + f^*(\pi - \theta) \exp(-ikr)/r. \end{aligned} \quad (3)$$

Without the scattered waves,  $f=0$ , the expression (1) reduces to the plane-wave Born-approximation amplitude. In practice the distorted waves are generated from an optical-model potential  $U(r)$  which reproduces the observed elastic scattering from the same nucleus at the same energy, and thus satisfy the Schrödinger equation

$$[\nabla^2 + k^2 - (2\mu/\hbar^2)U(r) - (2\mu/\hbar^2)U_c(r)]\chi(\mathbf{k}, \mathbf{r}) = 0, \quad (4)$$

where  $U_c$  is the Coulomb potential. For a uniformly charged sphere of radius  $R_c$ ,

$$\begin{aligned} (2\mu/\hbar^2)U_c &= 2kn/r & \text{if } r > R_c, \\ &= (kn/R_c)[3 - (r^2/R_c^2)] & \text{if } r \leq R_c. \end{aligned} \quad (5)$$

The reduced mass of the colliding pair is  $\mu$ , and  $n$  is the Coulomb parameter  $ZZ'\mu e^2/\hbar^2 k$  if  $Z$  and  $Z'$  are the charge numbers of target and projectile, respectively.

<sup>6</sup> A. Bohr, *Physica* **22**, 963 (1956); B. L. Cohen and A. G. Rubin, *Phys. Rev.* **111**, 1568 (1958); W. T. Pinkston and G. R. Satchler, *Nuclear Phys.* **27**, 270 (1961).

The remaining factor in the amplitude (1) is the matrix element of the interaction causing the inelastic transition, taken between the *internal* states of the colliding pair. It plays the role of an effective interaction for scattering from one elastic scattering state to another, and contains all the information on nuclear structure, angular momentum, selection rules, etc. However, we do assume the interaction is static and nonexchange. We also neglect contributions from exchange between projectile and target due to (anti) symmetrization.

Here we are interested in alpha particles, which have no spin, so a general (static) interaction can be written  $V(\mathbf{r}, \xi)$ , where  $\xi$  represents the internal coordinates of the target. Expanded into multipoles<sup>7</sup> this becomes

$$V(\mathbf{r}, \xi) = \sum_{lm} V_{lm}(r, \xi) [i^l Y_l^m(\Theta, \Phi)]^*, \quad (6)$$

where  $(\Theta, \Phi)$  are the polar angles of  $\mathbf{r}$ . Since  $V$  is scalar, the  $V_{lm}$  must behave under rotations of coordinates like the spherical harmonics  $Y_l^m$ , and have parity  $(-)^l$ . The factor  $i^l$  is included to ensure the reality of nuclear reduced matrix elements.<sup>7</sup> Inverted, Eq. (6) gives

$$V_{lm}(r, \xi) = i^l \int \int V(\mathbf{r}, \xi) Y_l^m(\Theta, \Phi) \sin\Theta d\Theta d\Phi.$$

Applying the Wigner-Eckart theorem<sup>7</sup> to the matrix elements of the interaction (6), we get for the effective interaction in Eq. (1),

$$\begin{aligned} \langle J_f M_f | V | J_i M_i \rangle &= \sum_l \langle J_f M_f | J_l M_l | J_i M_i \rangle \\ &\times \langle J_f || V_l || J_i \rangle [i^l Y_l^m(\Theta, \Phi)]^*, \end{aligned} \quad (7)$$

where  $J_i, J_f$  are the initial and final nuclear spins, and  $M_i, M_f$  are their  $z$  components. We then see the  $l$ th multipole in the expansion (6) corresponds to transfer of angular momentum  $l$  to the target nucleus. The Clebsch-Gordan coefficient ensures conservation of angular momentum,

$$|J_i - J_f| \leq l \leq J_i + J_f, \quad (8)$$

while the spherical harmonic determines the change in parity to be  $(-)^l$ . The reduced matrix element is now a function of radius only, and it is convenient to write it as the product of a "strength" times a "form factor,"

$$\langle J_f || V_l || J_i \rangle = A_l F_l(r). \quad (9)$$

This separation is one of convenience, so that, for example, universal form factors with simple normalization may be used in computation. Those suggested by the collective model are discussed in the next section. However, we may say quite generally that  $F_l(r)$  goes to zero as  $r$  becomes large, and is also zero at the origin for nonzero  $l$ .

To evaluate the amplitude (1), we need the partial-wave expansion of the distorted waves

$$\begin{aligned} \chi^{(+)}(\mathbf{k}, \mathbf{r}) &= (4\pi/kr) \sum_L i^L \chi_L(kr) \\ &\times \sum_M Y_L^M(\Theta, \Phi) Y_L^{M*}(\theta, \phi), \end{aligned} \quad (10)$$

<sup>7</sup> D. M. Brink and G. R. Satchler, *Angular Momentum* (Oxford University Press, New York, 1962).

together with the time-reversal relation<sup>2</sup>

$$\chi^{(-)*}(\mathbf{k}, \mathbf{r}) = \chi^{(+)}(-\mathbf{k}, \mathbf{r}). \quad (11)$$

In Eq. (10) the polar angles of  $\mathbf{k}$  are denoted by  $(\theta, \phi)$ . The distorted partial wave  $\chi_L$  then satisfies the radial equation

$$\left[ \frac{d^2}{dr^2} + k^2 - L(L+1)/r^2 - (2\mu/\hbar^2)U(r) - (2\mu/\hbar^2)U_c(r) \right] \chi_L(kr) = 0, \quad (12)$$

with the boundary condition  $\chi_L(0) = 0$ . Beyond the range of the potential  $U(r)$  it has the form

$$\chi_L = (i/2)(H_L^* - \eta_L H_L) \exp(i\sigma_L), \quad (13)$$

where  $H_L = G_L + iF_L$  is the outgoing-wave Coulomb function,<sup>8</sup> and  $\eta_L$  is the reflection coefficient as defined by Blatt and Weisskopf.<sup>9</sup> Then asymptotically

$$\chi_L \rightarrow (i/2) [\exp(-i\theta_L) - \eta_L \exp(i\theta_L)] \exp(i\sigma_L),$$

where

$$\begin{aligned} \theta_L &= kr - n \ln(2kr) - (l\pi/2) + \sigma_L, \\ \sigma_L &= \arg\Gamma(L+1+in). \end{aligned}$$

The differential cross section for elastic scattering corresponding to these distorted waves is then<sup>9</sup>

$$(d\sigma_{el}/d\Omega) = |f_c(\theta) + f_n(\theta)|^2, \quad (14)$$

where the Coulomb scattering amplitude is

$$f_c(\theta) = -(n/2k) \csc^2(\theta/2) \exp[-2in(\ln \sin \frac{1}{2}\theta - \sigma_0)], \quad (15)$$

and the additional amplitude induced by the optical potential  $U(r)$  is

$$f_n(\theta) = -(2ik)^{-1} \sum_L (2L+1)(1-\eta_L) \times \exp[2i\sigma_L] P_L(\theta). \quad (16)$$

When the expansions (6) and (10) are inserted into the amplitude (1), the integrations over  $\Theta$  and  $\Phi$  may be carried out. With the  $z$  axis along the incident direction  $\mathbf{k}_i$  and the  $y$  axis along  $\mathbf{k}_i \times \mathbf{k}_f$  the result may be written

$$T_{fi} = [(4\pi)^{1/2}/k_f^2] \sum_l A_l \langle J_f M_f | J_i M_i m \rangle \times (2l+1)^{1/2} \beta^{lm}(\theta), \quad (15)$$

where the amplitude for transfer of angular momentum  $l$  with  $z$  component  $m$  is

$$\beta^{lm} = (-)^m \beta^{l-m} = \sum_{L'L} \Gamma_{L'L}^{lm} P_{L'}^m(\theta) f_{L'L}^l, \quad m \geq 0. \quad (16)$$

The radial integrals are given by

$$f_{L'L}^l = \frac{k_f}{k_i} \int \chi_{L'}^{(f)}(k_f r) F_l(r) \chi_L^{(i)}(k_i r) dr, \quad (17)$$

<sup>8</sup> M. Hull and G. Breit, *Encyclopedia of Physics*, edited by S. Flügge (Springer-Verlag, Berlin, 1959), Vol. 41.

<sup>9</sup> J. M. Blatt and V. F. Weisskopf, *Theoretical Nuclear Physics* (John Wiley & Sons, Inc., New York, 1952), Chap. VIII.

and the gamma coefficients result from integrating over the three spherical harmonics,

$$\Gamma_{L'L}^{lm} = i^{L-L'} (2L'+1) [(L'-m)!/(L'+m)!]^{1/2} \times \langle L'00 | L0 \rangle \langle L'm-m | L0 \rangle; \quad m \geq 0. \quad (18)$$

In this form the differential cross section for scattering through the angle  $\theta$  becomes, after summing over  $M_f$  and averaging over  $M_i$ ,

$$d\sigma/d\Omega = [(2J_f+1)/(2J_i+1)] \sum_l |A_l|^2 \sigma_l(\theta), \quad (19a)$$

where the "reduced" cross section is given by

$$\sigma_l(\theta) = (\mu^2/k_f^3 k_i \pi \hbar^4) \sum_m |\beta^{lm}(\theta)|^2. \quad (19b)$$

Some previous calculations<sup>1,2</sup> have used simplifying assumptions in the evaluation of the integrals (17), in particular the surface approximation which replaces the integral by the value of the integrand at the nuclear surface. When this is done, some other procedure has to be used to obtain the correct normalization of the results. Comparison between the results of this surface approximation and the full calculation will be made in the following paper.

### III. COLLECTIVE MODEL FORM FACTORS

The collective model of the nucleus attributes many low-lying excited states to oscillations in shape about a spherical mean (vibrations), or to the rotations of a statically deformed shape.<sup>10</sup> This leads naturally to an extension of the optical model to include nonspherical potentials, in the same way that deformed shell-model potentials are used to generate the bound states of nucleons in these nuclei. The nonspherical parts of the potential are then able to induce inelastic scattering to these collective vibrational or rotational states. This model has the advantage that the parameters for the radial form factor are determined by the optical model for the *elastic* scattering; all that remains is a strength (or deformation) to be extracted by comparison with the experimentally observed inelastic cross section. The success of this model has to be judged in two ways. First, does it reproduce the shape of the angular distribution correctly? In general, this tests the correctness of the radial form factor chosen, although we shall see that for alpha particles, because of their strong absorption, the angular distribution is insensitive to the form factor shape. When absorption is strong, the significant contributions to the reaction tend to arise only from the region just outside the nucleus where the tails of acceptable form factors tend to be rather similar. Secondly, is the interaction strength or deformation required to fit the measured cross section consistent with those found by other techniques such as measurement of the electric quadrupole moment and Coulomb excitation? These questions will be studied below and in the following paper.

<sup>10</sup> A. Bohr and B. Mottelson, *Kgl. Danske. Videnskab. Selskab, Mat.-fys. Medd.* **27**, No. 16 (1953).

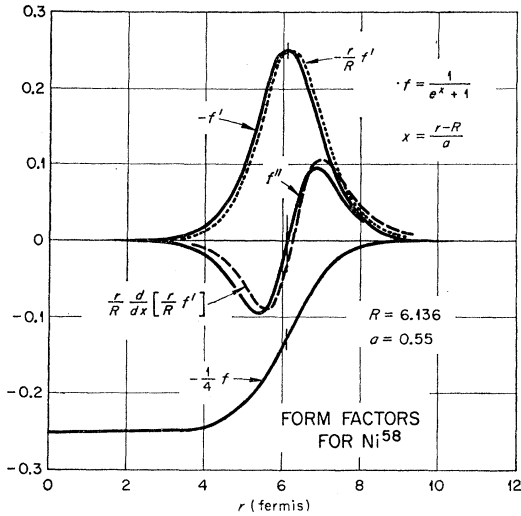


FIG. 1. Collective-model radial form factors for inelastic scattering. The function  $f(x)$  is the usual Woods-Saxon optical-potential form factor, and the derivatives are those appearing in the expansions (23) and (30).

### A. Rotational Excitation

We derive the interaction from a deformed, or non-spherical potential well. It is reasonable to assume the potential strength depends only on the distance  $(r-R)$  from the surface, and then allow this surface to be nonspherical,

$$R(\Theta', \Phi') = R_0 \left[ 1 - \sum_{kq} |\alpha_{kq}|^2 / 4\pi + \sum_{kq} \alpha_{kq} Y_{kq}(\Theta', \Phi') \right]. \quad (20)$$

The volume enclosed by this surface is constant to second order in the deformation. The polar angles  $(\Theta', \Phi')$  are referred to the body-fixed principal axes of the nucleus. For a quadrupole deformation,  $k=2$ , and in terms of the familiar<sup>10</sup> deformation parameter  $\beta$  and asymmetry parameter  $\gamma$  we have

$$\alpha_{20} = \beta \cos \gamma; \quad \alpha_{2\pm 1} = 0; \quad \alpha_{2\pm 2} = \beta \sin \gamma / \sqrt{2}. \quad (21)$$

Axial symmetry would require  $\gamma=0$ .

We then take the potential  $U \equiv U[r-R(\Theta', \Phi')]$ . The much used Woods-Saxon potential shape is of this type

$$U(x) = -U_0 / (e^x + 1), \quad x = (r-R)/a. \quad (22)$$

A Taylor-series expansion about  $R=R_0$  yields

$$U(r-R) = U(r-R_0) - \delta R (d/dr)U(r-R_0) + \frac{1}{2}(\delta R)^2 (d^2/dr^2)U(r-R_0), \quad (23)$$

where

$$\delta R = R_0 \left[ \sum_{kq} \alpha_{kq} Y_{kq}(\Theta', \Phi') - \sum_{kq} |\alpha_{kq}|^2 / 4\pi \right]. \quad (24)$$

The scalar first term we identify with the spherical optical potential used to describe the elastic scattering (and generate the distorted waves). The other terms we may identify with the inelastic interaction (6) (except for some second-order corrections to the elastic

potential). We note that on this model a given multipole deformation  $k$  of the surface  $R(\Theta, \Phi)$  in first order gives the interaction term  $V_l$  with  $l=k$ , but in second and higher orders it contributes to other multipole terms in the interaction (6). In second order, for example, it contributes to all even values of  $l$  in the range  $0 \leq l \leq 2k$ . However, it would be inconsistent to use the interaction (23) expanded to second order in the deformation while only calculating the transition amplitude to first order in the interaction, unless one could show the second-order contributions of the first-order interaction were negligible. On the contrary, however, it appears that these terms are at least comparable to the first-order contributions of the second-order interaction potential.<sup>11</sup>

The expression (20) for the deviation from spherical shape is still referred to body-fixed axes; we must rotate into a space-fixed coordinate system, using

$$Y_{kq}(\Theta', \Phi') = \sum_{q'} Y_{kq'}(\Theta, \Phi) D_{q'q}^k(R^{-1}), \quad (25)$$

where  $R$  is the rotation taking the body-fixed axes into coincidence with the space-fixed axes.<sup>7</sup> Comparison of Eq. (23) with Eq. (6) then gives the first-order interaction term

$$V_{lm} = -i^l R_0 [dU(r-R_0)/dr] \sum_q \alpha_{lq}^* D_{qm}^l(R). \quad (26)$$

For an axially-symmetric deformation this may be written

$$V_{lm} = -i^l R_0 \beta_l (4\pi/2l+1)^{1/2} (dU/dr) Y_l^m(\beta, \alpha), \quad (27)$$

where  $(\beta, \alpha)$  are the polar angles of the nuclear symmetry axis.

If we take the Woods-Saxon form (22) for the central optical potential  $U(r-R_0)$ , then with  $x = (r-R_0)/a$ ,

$$dU/dr = (dU/dx)/a = (U_0/a) e^x / (e^x + 1)^2, \quad (28)$$

which peaks at  $r=R_0$  and has a width at half-maximum of  $3.5a$  (see Fig. 1).

An alternative way to define the potential  $U(r, \Theta', \Phi')$  is in terms of equipotential surfaces which conserve volume (to second order),

$$r' = r \left[ 1 + \sum_{kq} |\alpha_{kq}|^2 / 2\pi - \sum_{kq} \alpha_{kq} Y_{kq}(\Theta', \Phi') \right], \quad (29)$$

so that the Taylor series becomes

$$U(r') = U(r) + \delta r dU(r)/dr + \frac{1}{2}(\delta r)^2 d^2U(r)/dr^2 \dots, \quad (30)$$

where

$$\delta r = -r \left[ \sum_{kq} \alpha_{kq} Y_{kq}(\Theta', \Phi') - \sum_{kq} |\alpha_{kq}|^2 / 2\pi \right].$$

Thus, the only effect is to replace the  $R_0$  of Eqs. (26) and (27) by  $r$ , which gives the interactions a slightly longer tail (Fig. 1).

It now remains to calculate the nuclear matrix elements of the interaction (26). We shall only consider scattering from even nuclei in detail; the extension to odd nuclei is straightforward. The wave functions for

<sup>11</sup> B. Buck, Phys. Rev. **127**, 940 (1962).

an asymmetric rotator may be written<sup>12</sup>

$$\psi_{\alpha JM} = \sum_K A_K \alpha \psi_{KJM}, \quad (31)$$

where

$$\psi_{KJM} = \left[ \frac{2J+1}{16\pi^2(1+\delta_{K,0})} \right]^{1/2} \times [D_{KM}^J(R) + (-)^J D_{-KM}^J(R)].$$

The (real) mixing coefficients  $A$  have been given in reference 12; for axially symmetric nuclei only  $K=0$  and even  $J$  enter, and  $A_0=1$ . The interaction (26) can be written

$$V_{lm} = \sum_{\mu} \bar{V}_{l\mu} D_{\mu m}^l(R). \quad (32)$$

For even target nuclei we have  $J_i=K_i=0$ , and therefore  $J_f=l$  only, with the matrix elements

$$\langle J_f=l || V_l || J_i=0 \rangle = \left[ \frac{2}{2l+1} \right]^{1/2} \sum_{K_f} \frac{A_{K_f} \bar{V}_{lK_f}}{(1+\delta_{K_f,0})^{1/2}}. \quad (33)$$

In the axially symmetric case, with  $K_f=0$  only, this is just

$$\langle J_f=l || V_l || J_i=0 \rangle = \bar{V}_{l0} / (2l+1)^{1/2}. \quad (34)$$

Similarly, excitation of levels in the ground-state rotational band of axially-symmetric odd nuclei has matrix elements

$$\langle KJ_f || V_l || KJ_i \rangle = \bar{V}_{l0} \langle J_i K | J_f l K 0 \rangle (-)^{J_i-J_f}. \quad (35)$$

These matrix elements may be put in the separated form of Eq. (9). For example, for axially symmetric even nuclei, and using the Woods-Saxon potential (28), we may write

$$A_l = i^l (2l+1)^{-1/2} (\beta_l R_0 U_0 / a), \quad (36)$$

$$F_l(r) = (d/dx)(e^x + 1)^{-1}. \quad (37)$$

### B. Vibrational Excitations

The interaction model adopted here is the same as for rotations, namely, a nonspherical potential well, except the shape is no longer static but oscillates about a spherical mean. This is simply achieved by treating the deformation parameters  $\alpha_{kq}$  in Eq. (20) as dynamical variables,<sup>10</sup>

$$\alpha_{kq} = (\hbar\omega_k / 2C_k)^{1/2} [b_{kq} + (-)^q b_{k-q}^*] = (-)^q \alpha_{k-q}^*, \quad (38)$$

where the  $b_{kq}$  and  $b_{kq}^*$  are the usual boson annihilation and creation operators for a  $2^k$ -pole oscillation with angular momentum  $k$  and  $z$  component  $q$ . The energy of each phonon is  $\hbar\omega_k$ , and  $C_k$  is the restoring-force parameter. Since the deformation is no longer static, the expressions (20), (24), and (26) may now be regarded as referring to space-fixed coordinates. Using the Taylor

expression just as before, to first order we have

$$V_{lm} = i^l R_0 [dU(r-R_0)/dr] \alpha_{lm}^*. \quad (39)$$

We only discuss excitation of even target nuclei, but the extension to odd nuclei is straightforward. The target then has zero spin, with no phonons present. The interaction (39) is able to excite a single  $2^l$ -pole phonon with a matrix element

$$\langle J_f=l || V_l || J_i=0 \rangle = -i^l R_0 [dU(r-R_0)/dr] (\hbar\omega_l / 2C_l)^{1/2}. \quad (40)$$

This may be written in a form analogous to Eqs. (36) and (37) with

$$A_l = i^l (R_0 U_0 / a) (\hbar\omega_l / 2C_l)^{1/2}. \quad (41)$$

Clearly then the phonon transition strength is the same as for rotational excitation with an equivalent deformation  $\beta_l$ . This is just the root mean square deformation in the ground state due to zero-point oscillations,

$$\beta_l^2 = \langle \sum_m |\alpha_{lm}|^2 \rangle = (2l+1) (\hbar\omega_l / 2C_l). \quad (42)$$

### IV. NUMERICAL CALCULATIONS

In principle, the analysis of experimental data using the model described here first attempts to find an optical potential which describes the observed elastic scattering. This is conveniently done by the use of an automatic search routine which adjusts the potential parameters until the mean square deviation of the predictions from the observed cross sections is a minimum.<sup>13</sup> These parameters are then used in the distorted-wave calculation to predict the shapes of the inelastic angular distributions. The magnitude of the experimental cross section for a given transition then determines the square of the corresponding nuclear deformation.

In the present paper only an example of this procedure is given; our main purpose is to study the behavior of typical cases and the effects of varying the parameters. The interpretation of some of these results is discussed in the following paper,<sup>14</sup> while a detailed analysis of available experimental data will be published later.

Previous distorted-wave calculations of alpha-particle scattering have employed the surface approximation for the radial integrals.<sup>2</sup> However, even these are impractical without the aid of high-speed computers if more than a few are to be done, and currently available computing facilities are fast enough to make the complete calculation feasible. The calculations reported here were carried out using the Oak Ridge distorted-wave code.<sup>15</sup> A typical case of the inelastic scattering of 40-MeV alpha particles, using 30 partial waves, takes about

<sup>13</sup> R. M. Drisko and R. H. Bassel (unpublished).

<sup>14</sup> E. Rost, following paper [Phys. Rev. **128**, 2708 (1962)].

<sup>15</sup> R. H. Bassel, R. M. Drisko, and G. R. Satchler, Oak Ridge National Laboratory Report No. 3240 (unpublished).

<sup>12</sup> A. S. Davydov and G. F. Filippov, Nuclear Phys. **8**, 237 (1958); A. S. Davydov and V. S. Rostovsky, *ibid.* **12**, 58 (1959).

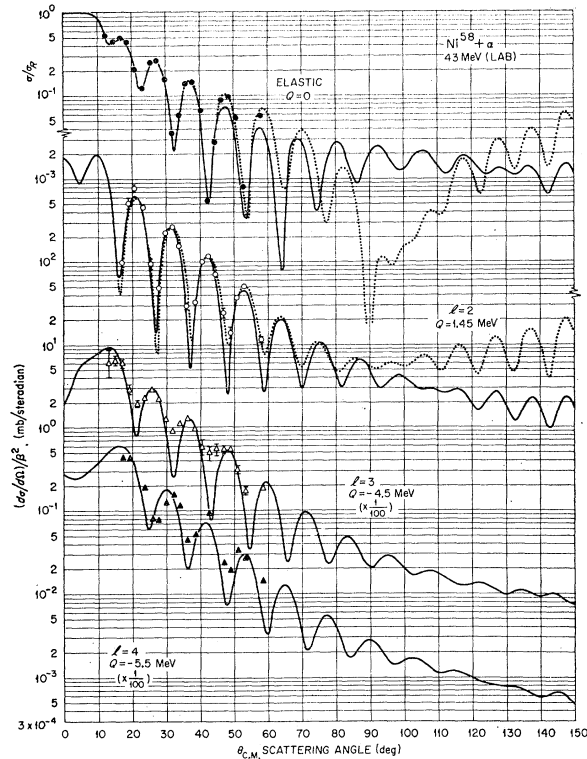


FIG. 2. Angular distributions for the scattering of 43-MeV alphas from  $\text{Ni}^{58}$ . The parameters used are described in the text; a reaction cross section of 1.51 b is predicted by the optical potential corresponding to the full curve, and 1.50 b for the dashed curve. The experimental points are taken from reference 16.

4 min on the IBM-704, or about 40 sec on the IBM-7090, to compute a complete angular distribution.

### A. Typical Results

Figure 2 shows the results for 43-MeV alphas on  $\text{Ni}^{58}$ ; the theoretical curves were calculated at intervals of  $1^\circ$ , and the experimental values were obtained at Argonne National Laboratory.<sup>16</sup> At the time these calculations were made, elastic scattering data were only available for angles less than  $45^\circ$ . More than one set of optical potential parameters were found to give a good fit to these data; the theoretical curves for two of these are shown in Fig. 2. It will be seen that the two sets make significantly different predictions for wide-angle scattering, for which no experimental data are available. Fitting to the more complete elastic data which now extends to  $60^\circ$  leads to slight changes in the optical-model parameters, but these have very little effect on the inelastic predictions, and for the calculations reported here the original potentials were used. These were

<sup>16</sup> H. W. Broek, T. H. Braid, J. L. Yntema, and B. Zeidman, Phys. Rev. **127**, 1514 (1962). We are indebted to these authors for making their data available before publication.

based on the Woods-Saxon shape,

$$U(r) = -V(e^x + 1)^{-1} - iW(e^{x'} + 1)^{-1}, \quad (43)$$

$$x = (r - r_0 A^{1/3})/a, \quad x' = (r - r_0' A^{1/3})/a'.$$

The full-line curves in Fig. 2 were calculated with  $r_0 = r_0' = 1.585$  F,  $a = a' = 0.549$  F,  $V = 47.6$  MeV, and  $W = 13.8$  MeV. The broken curves used a potential for which the absorptive part has a different shape from the real part,  $r_0 = 1.5$  F,  $r_0' = 1.02$  F,  $a = 0.517$  F,  $a' = 0.809$  F,  $V = 96.7$  MeV, and  $W = 38.2$  MeV.

The three inelastic angular distributions shown in Fig. 2 were calculated using the derivative of the real part of the optical potential in the interaction (26) or (39). (The effects of including the imaginary part are discussed later.) The agreement with experiment is seen to be acceptable, and the magnitudes of the measured cross sections correspond to deformations  $\beta_l$  of 0.18 ( $l=2$ ), 0.14 ( $l=3$ ), and 0.06 ( $l=4$ ). The value of  $\beta_2$  is in good agreement with the quadrupole deformation deduced from Coulomb excitation measurements. For the  $l=2$  transition, results are presented for both optical potentials, and are very similar at angles for which experimental data are available. Although not shown, the same result is found for the  $l=3$  and  $l=4$  transitions. In particular, both optical potentials lead to the same values of the deformations, which suggests that optical potentials which are equivalent with respect

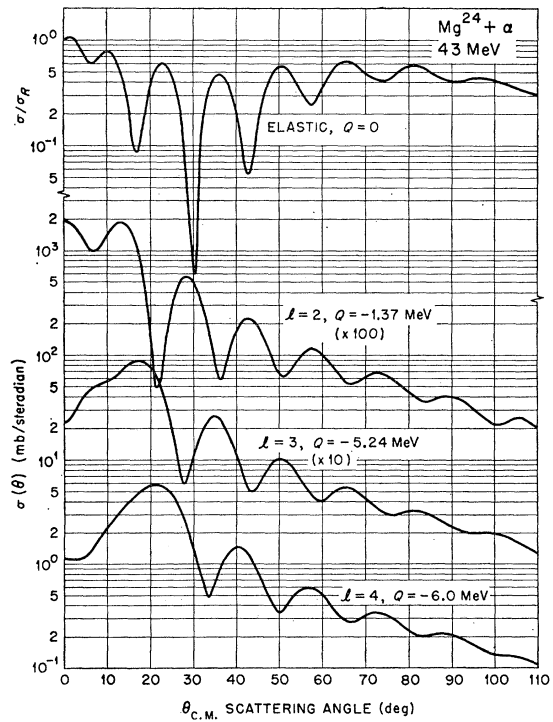


FIG. 3. Representative angular distributions for 43-MeV alphas on  $\text{Mg}^{24}$ . The same optical-potential parameters were used as for the solid curves in Fig. 2; they predict a reaction cross section of 1.07 b. The observed scattering from Mg requires a slightly larger radius of approximately  $r_0 = 1.65$ .

to the elastic scattering also predict the same inelastic scattering.

To give a feeling for the variation with nuclear size, the curves in Fig. 3 for  $\text{Mg}^{24}$  and Fig. 4 for  $\text{Zr}^{90}$  were computed using the same optical potential parameters as were used for the solid curves in Fig. 2. Some general features are evident in these figures which are characteristic of the scattering of medium-energy alpha particles. For example, the parity phase rule for the strongly oscillatory parts of the angular distributions,<sup>4</sup> the transitions with the change of parity ( $l$  odd) show oscillations in phase with the elastic, while those with no change of parity ( $l$  even) are out of phase with the elastic. The cross section at small angles also shows a parity dependence; the even-parity transitions tend to show a rise in intensity near  $0^\circ$ , while the odd-parity cross sections tend to zero. This behavior may be understood in terms of a symmetry property of the distorted-wave transition amplitude<sup>17</sup>; for zero energy loss (adiabatic limit), the odd-parity cross section should be identically zero at  $0^\circ$ . Another general feature is that

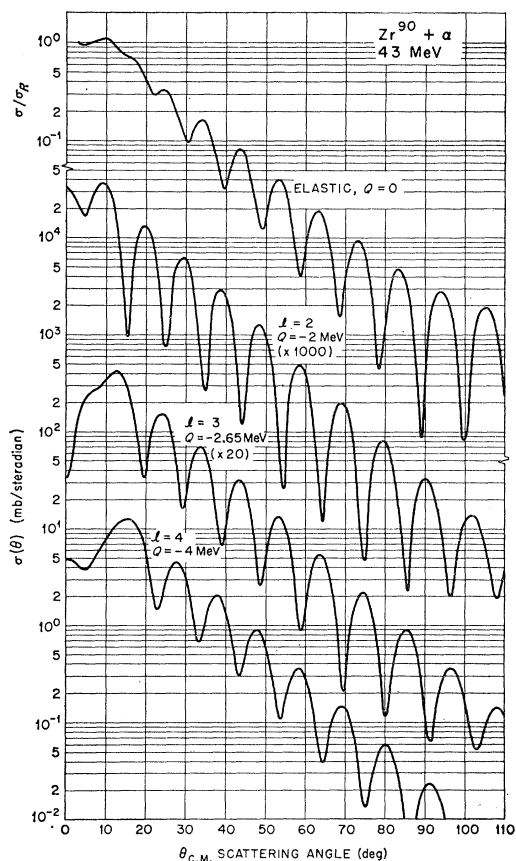


FIG. 4. Representative angular distributions for 43-MeV alphas on  $\text{Zr}^{90}$ . The same optical-potential parameters were used as for the solid curves in Fig. 2; they predict a reaction cross section of 1.77 b.

<sup>17</sup> A. J. Kromminga and I. E. McCarthy, Phys. Rev. Letters **6**, 62 (1961).

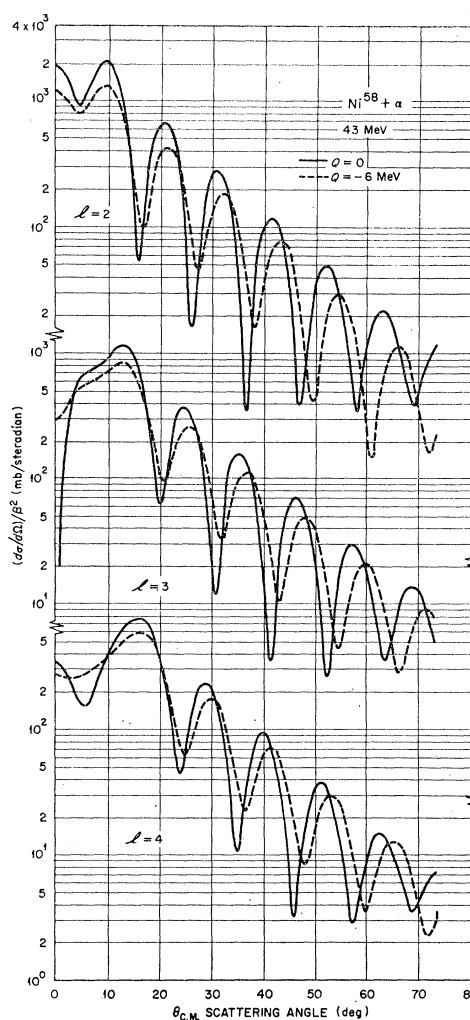


FIG. 5. Variations with  $Q$  value in the angular distributions of 43-MeV alphas on  $\text{Ni}^{58}$ . The same optical-potential parameters were used as for the solid curves in Fig. 2.

the oscillations are very evenly spaced in angle.<sup>2,18</sup> The angle between successive peaks decreases with increasing nuclear radius and is close to  $(\pi/kR_0)$ . This is about  $11^\circ$  for 43-MeV alphas on  $\text{Ni}^{58}$ . The amplitude of the oscillations becomes less marked for the large  $l$  values, and also falls off with increasing angle.

These features are somewhat dependent upon the energy loss during the scattering. This is illustrated for  $\text{Ni}^{58}$  in Fig. 5, where the predictions for  $Q=0$  and  $Q=-6$  MeV are compared. There is an over-all reduction in intensity for the nonadiabatic transitions, corresponding to the less perfect overlap between the initial and final distorted waves having different energies. For the same reason there is also a tendency for the minima in the angular distribution to be filled in for the nonadiabatic cases. However, the most significant difference probably

<sup>18</sup> L. Seidlitz, E. Bleuler, and D. J. Tendam, Phys. Rev. **110**, 682 (1958).

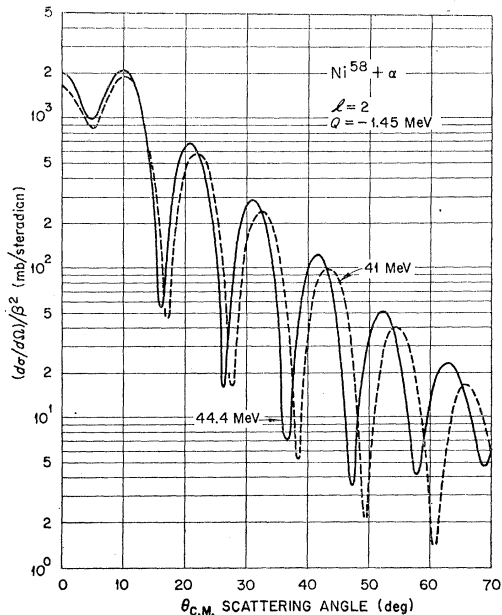


FIG. 6. Variation with bombarding energy of the angular distribution for the quadrupole transition in  $\text{Ni}^{58}$ . Other multipoles behave in a very similar way.

is the smooth shift of the diffraction structure to larger angles when there is energy loss. We have already mentioned the rule that the peaks are regularly spaced in angle by approximately  $(\pi/kR_0)$ . The shift with  $Q$  is consistent with this rule if we use for  $k$  the average of the initial and final wave numbers,  $k = \frac{1}{2}(k_i + k_f)$ . For  $Q=0$ ,  $k=k_i$ , while for  $Q=-6$  MeV at 43 MeV,  $k=0.96 k_i$ , thus leading to a 4% shift in angle. This is already  $2\frac{1}{2}^\circ$  at a scattering angle of  $60^\circ$ , so it is an appreciable fraction of the average spacing of  $11^\circ$  between peaks.

The effects of varying the bombarding energy (Fig. 6) are also well described by the  $(\pi/kR_0)$  rule for the spacing between peaks. Indeed, as has been noted before,<sup>4,5</sup> there is a strong tendency for the oscillatory parts of the angular distributions to have the form of universal curves when plotted against  $(kR_0\theta)$  rather than  $\theta$ . [One choice of shadow line in the Fraunhofer diffraction model<sup>4</sup> gives angular distributions which are oscillatory functions of  $2kR_0 \sin(\frac{1}{2}\theta)$ ; however, for the forward angles for which this model is valid, there is little difference between  $2 \sin(\frac{1}{2}\theta)$  and  $\theta$ .]

An example for a very light nucleus  $\text{Be}^9$  is shown in Fig. 7. The comparison with experiment<sup>19</sup> is somewhat preliminary since no great effort was made to find the optimum fit to the elastic data; however, the agreement already obtained is surprisingly good for such a light nucleus. If we assume that the 2.43-MeV level of  $\text{Be}^9$  is the  $J=5/2$  member of the  $K=3/2$  ground-state rotational band, the measured cross section corresponds to a deformation  $\beta_2=0.8$ . Figure 8 shows the result of a pre-

<sup>19</sup> R. G. Summers-Gill, Phys. Rev. **109**, 1591 (1958).

liminary analysis for 18-MeV alphas on  $\text{Ar}^{40}$ . The inelastic cross section corresponds to a deformation  $\beta_2=0.2$ ; however, it is clear the fit to the measured elastic angular distribution<sup>18</sup> is only qualitative. These curves for  $\text{Ar}^{40}$  are reproduced in Fig. 9 together with some for 18-MeV alphas on  $\text{Ne}^{20}$  and  $\text{Ni}^{58}$ . Although the main features of the angular distributions still remain, the diffraction structure is much less marked. In addition, for the heavier nuclei at this energy, Coulomb excitation is becoming important; indeed for Ni the Coulomb excitation cross section for the  $l=2$  transition is comparable to that for excitation by the specifically nuclear interaction. We return to a discussion of Coulomb excitation in Section V.

## B. Variation of Optical-Model Parameters

In this section we discuss the effects on the predictions for the inelastic scattering of changes in the parameters characterizing the optical potential. At the same time we vary the inelastic interaction parameters in the same way, so maintaining the correspondence with the optical potential given by Eqs. (26) and (39).

The reaction which has been studied most intensely is the scattering of 43-MeV alphas on  $\text{Ni}^{58}$ . However, the predictions of this model vary in a very smooth and simple way when we go to other nuclei and other energies, so that these results are typical of a wide range of reactions. The emphasis has also been on scattering angles in the forward hemisphere, since this is the region where most experimental data are available.

The "standard" set of parameters was taken to be those used in calculating the solid curves in Fig. 2. Then Figs. 10 through 13 show the results of changes of  $\pm 15\%$  in the real potential depth  $V$ ,  $\pm 30\%$  in the absorptive potential  $W$ ,  $\pm 10\%$  in the radius  $r_0$ , and  $\pm 20\%$  in the surface thickness  $a$ , respectively. Only the results for the  $l=2$  transition are shown. The effects on the  $l=3$  and 4 transitions have also been calculated

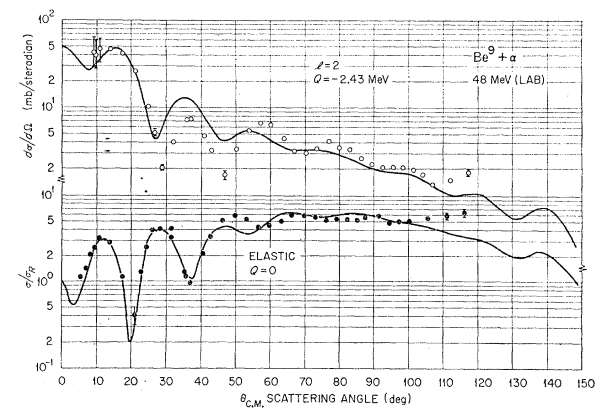


FIG. 7. Angular distributions for 48-MeV alphas on  $\text{Be}^9$ . The optical potential used was of Woods-Saxon form with  $V=69$  MeV,  $W=24$  MeV,  $r_0=1.57$  F,  $a=0.7$  F, which predicts a reaction cross section of 0.94 b. The experimental points are taken from reference 19.

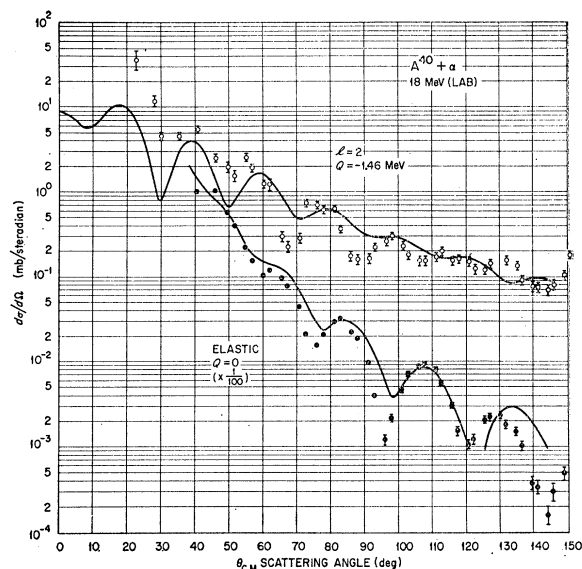


FIG. 8. Preliminary analysis for 18-MeV alphas on  $\text{Ar}^{40}$ . The optical potential is Woods-Saxon with  $V=45$  MeV,  $W=10$  MeV,  $r_0=1.7$  F,  $a=0.52$  F (these parameters were kindly supplied by F. G. J. Perey in private communication). The reaction cross section predicted is 1.14 barns. The experimental points are taken from reference 18.

and are very similar to those for  $l=2$ . In all cases, the phase relations with the elastic angular distributions are preserved.

The change when the radius is altered is closely what one would expect from keeping  $(kR_0\theta)$  constant, as has been observed in the previous section. The magnitude of the envelope to the oscillations of the cross section at forward angles increases roughly like  $R_0^2$ , as one would expect, but because the pattern is compressed for larger  $R_0$ , it also falls off with angle faster. Variation of  $V$  leads to little change except a slight shift of the pattern to larger angles for the weaker  $V$  and a corresponding slightly slower falloff with angle. Similarly, the large change in  $W$  has very little effect on the inelastic angular distributions. Reducing  $W$  fills in the diffraction minima somewhat and raises the cross section a little. The latter effect would be partly compensated for if the imaginary part of the optical potential had been included in the inelastic interaction, for the cross section would then be proportional to  $(V^2+W^2)$ .

Perhaps the most striking changes occur with variations in the surface thickness  $a$ . The peaks of the angular distribution shift with a change in  $a$  in a way similar to that for a fractional change in radius of roughly one quarter as much, while the magnitudes of the peak cross-sections increase with  $a$  about half as fast as with  $R$ . However, increasing  $a$  also tends to fill in the minima of the oscillations.

The interpretation of these results in terms of the angular momenta involved is discussed in the following paper.

### C. Variation of Form Factor

We now investigate the behavior of the angular distributions when the inelastic interaction form factor  $F(r)$  is changed while the optical potential is kept fixed. In this way we can see how the predictions would be affected by a failure of the simple deformed-potential model which relates the form factor to the optical potential.

The results are shown in Fig. 14 of using the expression (37) for the form factor, but using values of  $R_0$  and  $a_0$  different from those of the optical potential. Since the interaction strength need no longer be given by Eq. (36), the "reduced" cross sections  $\sigma(\theta)$  of Eq. (19b) are plotted. The transitions with  $l=3$  and  $l=4$  exhibit very similar behavior to those with  $l=2$ , so only the latter are illustrated. The main effect of giving the form factor a greater width ( $a_0$  larger) is to increase the magnitude of the cross section, although there is a slight shift in the positions of the peaks, and the peak magnitudes fall off somewhat faster with  $\theta$  for the larger  $a_0$ . Changing  $R_0$  again produces very little change in the peak positions, but the amplitude of the oscillations is reduced for the smaller  $R_0$ . However, there is a striking change in magnitude predicted; for example, the values of  $\sigma(\theta)$  at  $21^\circ$  are 0.33, 11.6, and 170 mb/sr when  $R_0$  is 5.14, 6.14, and 7.14 F, respectively; that is, a 500-fold increase in cross section for a 40% increase in  $R_0$ . This

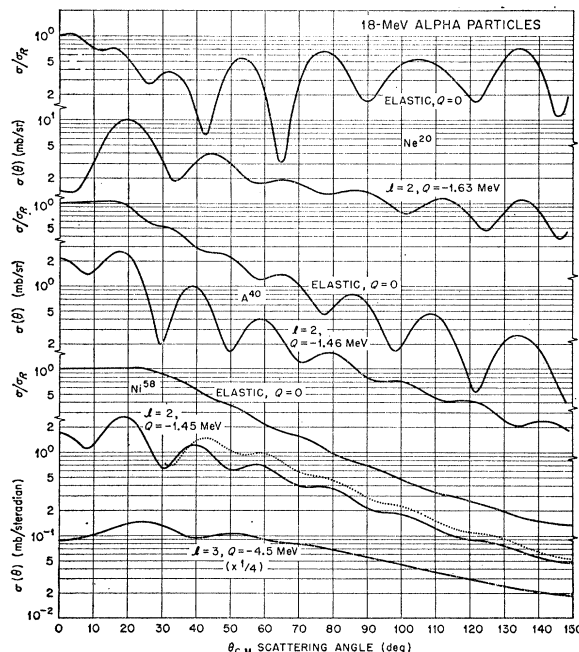


FIG. 9. Representative angular distributions for 18-MeV alphas. The curves for  $\text{Ar}^{40}$  are reproduced from Fig. 8, while those for  $\text{Ni}^{58}$  were calculated using the same parameters as the solid curves of Fig. 2. The optical potential used for  $\text{Ne}^{20}$  was Woods-Saxon with  $V=49$  MeV,  $W=6.5$  MeV,  $r_0=1.8$  F,  $a=0.53$  F. The reaction cross section predicted for Ni is 1.02 b, that for Ne is 1.12 b. The dashed curve for the quadrupole transition in Ni includes the effect of Coulomb excitation (see Fig. 16).

is to be contrasted to the behavior shown in Fig. 12 when the optical-potential radius is changed by the same amounts simultaneously. Then the average magnitude of  $\sigma(\theta)$  does not change (although  $d\sigma/d\Omega$  increases roughly as  $R_0^2$ ), but there are large shifts in the positions of the peaks. This suggests that the shapes of the inelastic angular distributions are determined primarily by the optical potential, while the details of the inelastic form factor mainly affect the magnitude of the cross section. This can be understood in terms of the localization of the reaction to a narrow region in the nuclear surface and the participation of a relatively small number of high partial waves, and will be discussed in the following paper.

Also, using the collective model (which determines the form factor parameters  $R_0$  and  $a_0$  to coincide with those of the optical potential) one obtains deformations from inelastic scattering which agree with those obtained by other means. The sensitivity of the magnitude of the cross section to changes in the form factor parameters implies this agreement would not occur unless the model were essentially correct.

The importance of the surface region is further emphasized by Fig. 15, in which volume and surface form

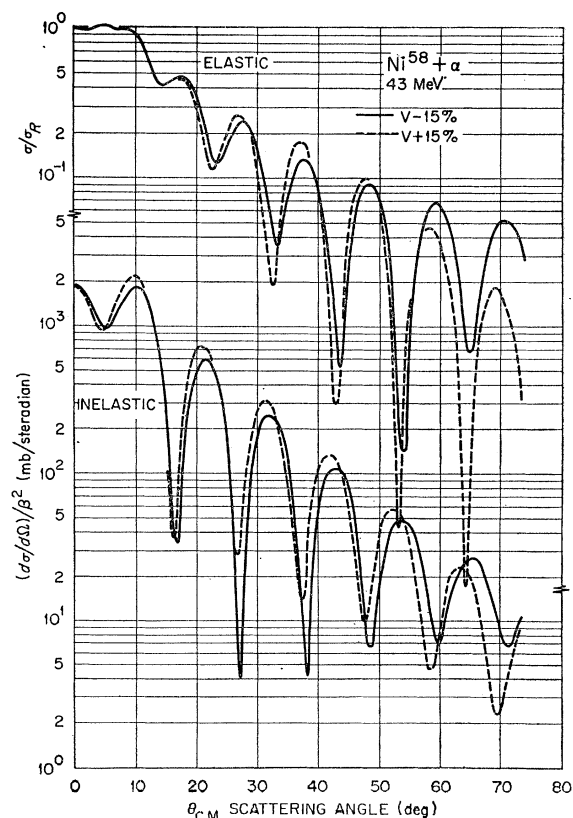


FIG. 10. Effects of varying the real potential well depth by  $\pm 15\%$ . Other parameters as for solid curves of Fig. 2. The corresponding reaction cross sections are 1.48 b for  $V-15\%$  and 1.54 b for  $V+15\%$ .

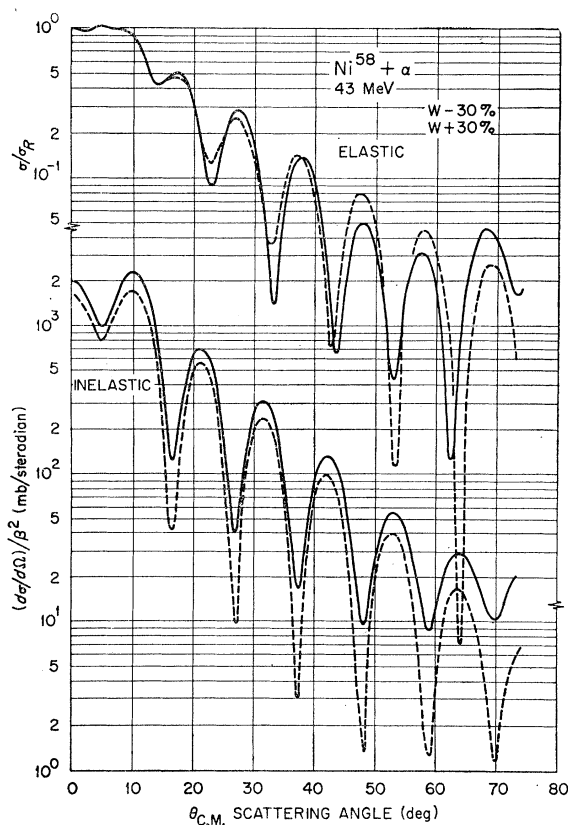


FIG. 11. Effects of varying the imaginary potential well depth by  $\pm 30\%$ . Other parameters as for solid curves of Fig. 2. The corresponding reaction cross sections are 1.49 b for  $W-30\%$  and 1.54 b for  $W+30\%$ .

factors are used. The volume interaction uses for  $F(r)$  the Woods-Saxon shape (22); the surface interaction is the standard one, Eq. (37), namely, the derivative of the volume interaction. Both use the values  $R_0=6.14$ ,  $a_0=0.55$  which are used for the optical potential. At forward angles the reduced cross sections predicted have very similar magnitudes, and are not too different in shape. Yet another example is afforded by Fig. 18, in which first- and second-derivative form factors (see Fig. 1) are compared; this example is discussed further in Sec. VI (b).

These results already suggest that there will be little change if we use the alternative way of defining the deformed potential well expressed by Eq. (29). Calculation has shown that this is so. The additional factor of  $r$  does increase  $F(r)$  slightly in the important region just outside the nuclear radius (see Fig. 1), and so enhances the cross section by roughly twice as much. If contributions to the scattering arose only from a definite radius  $R_{\text{eff}}$ , the cross section would be enhanced by  $(R_{\text{eff}}/R_0)^2$ . If  $R_{\text{eff}}$  were the radius required by the diffraction model, this factor is about 1.25 for  $\text{Ni}^{58}$  (with  $R_{\text{eff}}=6.83$ ). The calculated cross section is enhanced by about 1.6 at  $10^\circ$ , falling to 1.2 at backward angles. The shapes of the angular distributions are so similar

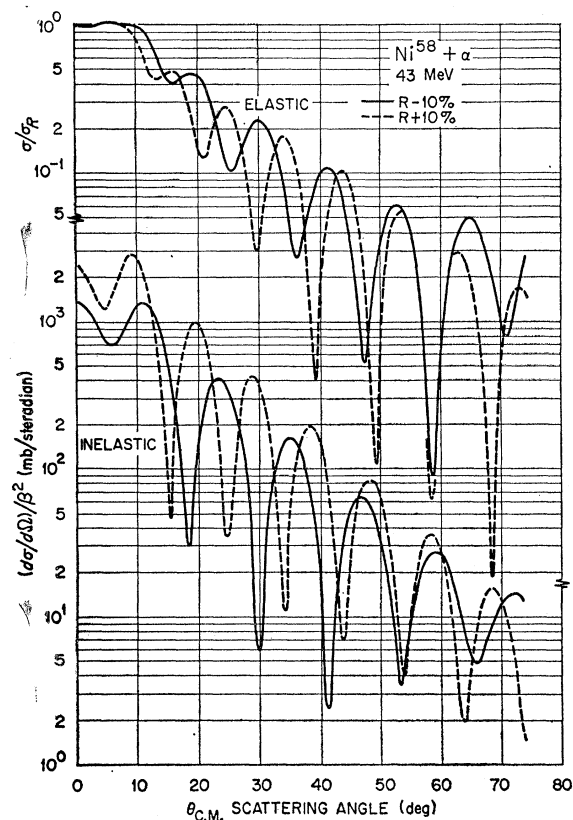


FIG. 12. Effects of varying the radius of the potential well by  $\pm 10\%$ . Other parameters as for the solid curves of Fig. 2. The corresponding reaction cross sections are 1.24 b for  $R-10\%$  and 1.81 b for  $R+10\%$ .

to those of Fig. 2 that it is not worth displaying them here; the main effect of using this form factor would be to reduce slightly the value of the deformation needed.

In conclusion, we see the general features of the angular distributions are rather insensitive to the shape of the form factor. However, their detailed behavior is affected somewhat by changes in the form factor, and it is possible that detailed analysis of precise experimental data will indicate whether the simple derivative form factor of Eq. (28) is adequate. In this connection it would be of interest to have experimental data for transitions in odd nuclei between different "single-particle" or intrinsic states, for which the interaction form factor is most likely to deviate from that of the simple deformed potential well.

### V. COULOMB EXCITATION

The inelastic scattering of charged particles is also accompanied by Coulomb excitation; indeed under some circumstances this is the main mode of excitation.<sup>20</sup> When both nuclear and Coulomb forces contribute, their amplitudes are coherent and interfere. We indicate

<sup>20</sup> K. Alder, A. Bohr, T. Huus, B. Mottelson, and A. Winther, *Revs. Modern Phys.* **28**, 432 (1956).

here how this Coulomb excitation may be included in distorted-wave approximation by modifying the interaction form factors, and present the results of some preliminary studies of its effects.

Since the calculation is carried out by partial-wave expansion, its accuracy is limited by the maximum value  $L_{\max}$  of angular momentum included. An associated restriction is imposed by the upper limit  $R_{\max}$  at which the radial integrals are cut off. This corresponds classically to omitting impact distances greater than  $R_{\max}$ , or neglecting angular momenta greater than  $\rho_{\max} = kR_{\max}$ . {More precisely, because of deflection of the trajectories by the Coulomb field, it corresponds to neglect of angular momenta greater than  $[\rho_{\max}(\rho_{\max} - 2n)]^{1/2}$ .} The classical deflection angle for angular momentum  $L_{\max}$  is  $\theta_c \approx 2n/L_{\max}$  if  $n \ll L_{\max}$ , so for scattering angles less than  $\theta_c$  the Coulomb excitation will be underestimated. At angles much greater than  $\theta_c$  the calculation should be accurate. For orientation we note that  $n=2.7$  for 43-MeV alphas on  $\text{Ni}^{58}$ , while  $n=4.2$  at 18 MeV. The present calculations were unable to use more than 50 partial waves; with these,  $\theta_c$  is about  $6^\circ$  at 43 MeV, and about  $10^\circ$  at 18 MeV. (For the purely nuclear interaction, no more than 30 partial waves are needed at 43 MeV, or about 20 at 18 MeV.)

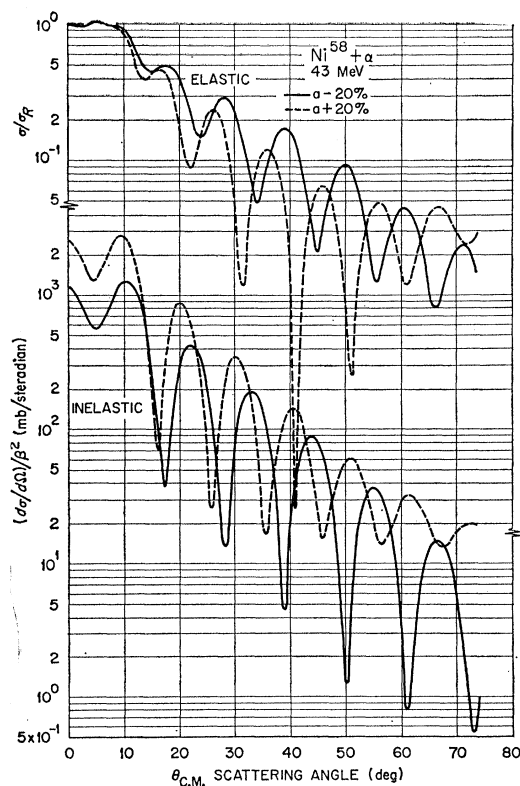


FIG. 13. Effects of varying the surface thickness of the potential well by  $\pm 20\%$ . Other parameters as for the solid curves of Fig. 2. The corresponding reaction cross sections are 1.39 b for  $a-20\%$  and 1.64 b for  $a+20\%$ .

The Coulomb interaction between target and projectile is

$$V^{(c)} = ZZ'e^2 \int \frac{\rho(\mathbf{r}')d\mathbf{r}'}{|\mathbf{r}-\mathbf{r}'|}$$

$$= \sum_{lm} \frac{4\pi ZZ'e^2}{2l+1} Y_{lm}^*(\Theta, \Phi) \times \int \frac{r_{<}^l}{r_{>}^{l+1}} Y_{lm}(\Theta', \Phi') \rho(\mathbf{r}') d\mathbf{r}', \quad (44)$$

where  $\rho(\mathbf{r})$  is the charge density normalized so that

$$\int \rho(\mathbf{r}) d\mathbf{r} = 1,$$

and  $r_{>}, r_{<}$  are the greater and lesser of  $r, r'$ . Eq. (44)

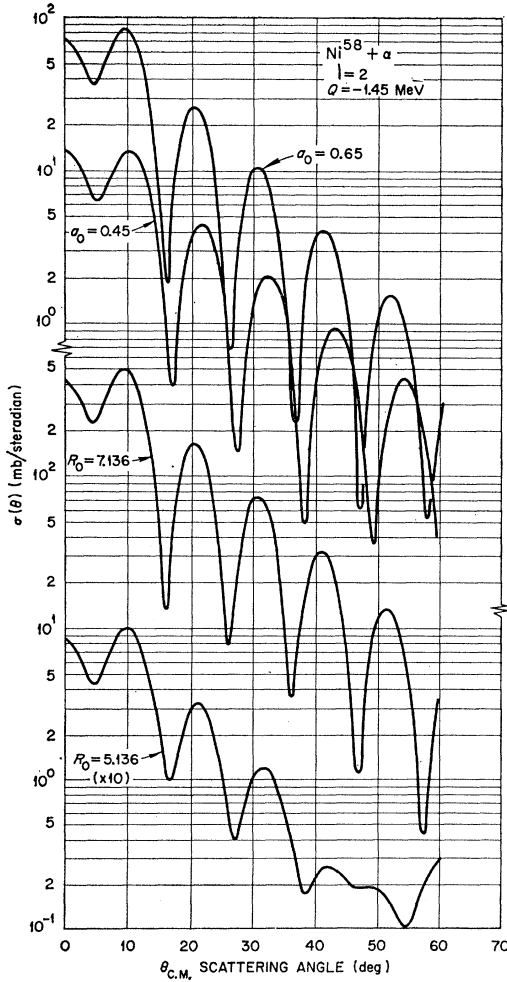


FIG. 14. Effects of varying the inelastic interaction form factor independently of the optical potential. Optical-potential parameters as for the solid curves of Fig. 2; these give  $R_0=6.136$  F,  $a_0=0.55$  F.

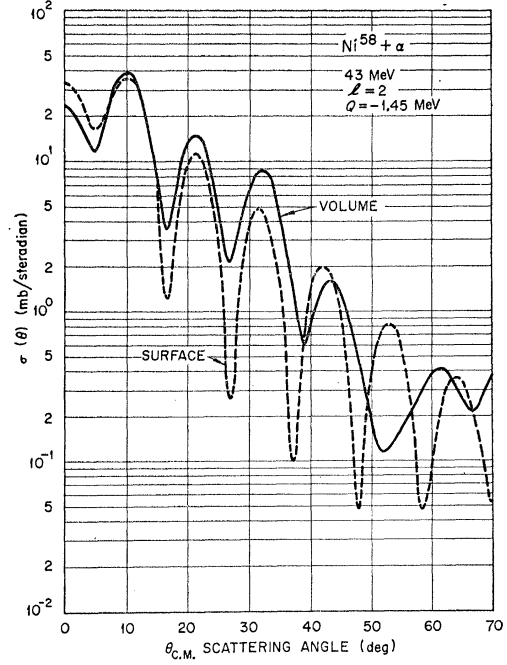


FIG. 15. Comparison of "volume" and "surface" interaction form factors. The volume form factor is of Woods-Saxon shape, and the surface form factor is the derivative of this. The parameters have the same values as for the solid curves of Fig. 2. While the volume interaction is unphysical, it serves to emphasize the relative unimportance of contributions from the nuclear interior.

has the form of the expansion (6) with

$$V_{lm}^{(c)}(r) = \frac{4\pi ZZ'e^2}{2l+1} i^l \int \frac{r_{<}^l}{r_{>}^{l+1}} \rho(\mathbf{r}') Y_{lm}(\Theta', \Phi') d\mathbf{r}'$$

$$= \frac{4\pi ZZ'e^2}{2l+1} \int \rho_{lm}(r') \frac{r_{<}^l}{r_{>}^{l+1}} r'^2 dr', \quad (45)$$

if

$$\rho(\mathbf{r}) = \sum_{lm} \rho_{lm}(r) [i^l Y_{lm}(\Theta, \Phi)]^*.$$

For values of  $r$  outside the nucleus (that is, where the charge density  $\rho$  is negligible),  $V_{lm}^{(c)}$  is proportional to  $r^{-l-1}$ , and Eq. (45) may be written

$$V_{lm}^{(c)}(r) = [4\pi Z'e/(2l+1)] [i^l/r^{l+1}] M_e(l, M), \quad (46)$$

where  $M_e(l, M)$  is the multipole operator for electric radiative transitions.<sup>10,20</sup> The well-known reduced transition probability is then just

$$B_{i \rightarrow f}(El) = |\langle i || M_e(l) || f \rangle|^2. \quad (47)$$

We can obtain expressions for the moments  $\rho_{lm}$  in the same way that we treated the deformed optical potential in Eq. (23). A simple example is a uniform charge distribution of radius  $R_c$ . To first order in the deformation we find

$$V_{lm}^{(c)}(r) = \frac{3ZZ'e^2 i^l}{2l+1} \alpha_{lm}^* \times \begin{cases} R_c^l/r^{l+1} & \text{if } r \geq R_c, \\ r^l/R_c^{l+1} & \text{if } r < R_c. \end{cases} \quad (48)$$

(A diffuse-edge charge distribution would round off the cusp in  $V_{lm}^{(c)}$  at  $r=R_c$ .) The Coulomb excitation may then easily be included in Eqs. (26) or (39) by modifying the radial form factor. If we neglect the interaction (45) inside  $R_c$ , and assume the charge density and optical potential have the same deformation, Eq. (37) becomes

$$F_l(r) = (d/dx)(e^x + 1)^{-1} + C_l r^{-l-1},$$

where

$$C_l = \begin{cases} 3(2l+1)^{-1} Z Z' e^2 R_c^l (a/R_0 U_0) & \text{if } r \geq R_c, \\ = 0 & \text{if } r < R_c. \end{cases} \quad (49)$$

This form was used for the calculations reported here. The neglect of Coulomb excitation contributions from  $r < R_c$  has been justified by explicit calculation with different values of  $R_c$ , but keeping  $C_l$  fixed.

Figure 16 shows that Coulomb excitation has little effect at 43 MeV when the target is Ni, except at very small angles. The effect on higher multipoles is even less. This is true generally because of the longer "tail" of the interaction for lower multipoles. At the lower energy of 18 MeV, however, the Coulomb excitation and its interference with the nuclear excitation has become important. Indeed Fig. 17 shows that the Coulomb excitation amplitude is already comparable to that from the purely nuclear interaction. Figure 16 also illustrates the importance of including sufficient partial waves in the calculation. At 18 MeV,  $\theta_c \approx 8.4/L_{\max}$ , so that Fig. 16 shows the Coulomb excitation contribution is calculated with reasonable accuracy for scattering angles greater than about  $3\theta_c$ .

Figure 17 shows the results of excitation at 18 MeV due to the Coulomb interaction (45) alone. The curves

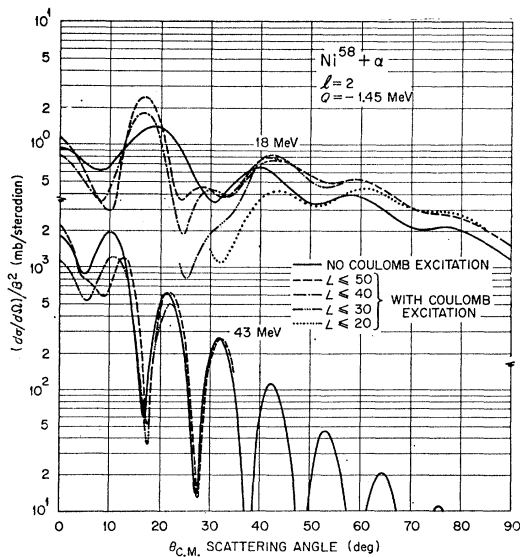


FIG. 16. Effects of including Coulomb excitation in the quadrupole transition in  $\text{Ni}^{58}$ . The parameter  $C_2$  of Eq. (49) is taken as 2.13. The various broken curves correspond to using different numbers of partial waves.

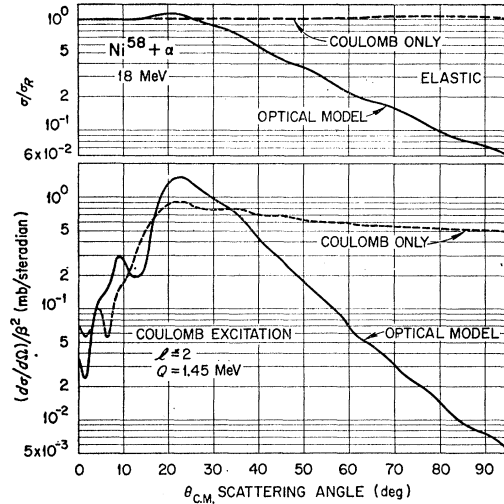


FIG. 17. Purely Coulomb excitation of Ni by 18-MeV alphas. The curve labeled "Coulomb only" use waves distorted only by the Coulomb potential from a uniform charge distribution of radius 6.14 F; those labeled "optical model" use waves distorted by an optical potential in addition. The optical-potential parameters are as for the solid curves of Fig. 2. The parameter  $C_2 = 2.13$ .

in Fig. 17 labeled "Coulomb only" were calculated with Coulomb distorted waves, but no optical potential, so may be directly compared with previous Coulomb excitation calculations. Fifty partial waves were used, so the results are probably accurate for  $\theta \gtrsim 25^\circ$ . We note that the finite-sized charge distribution used leads to very little departure of the elastic cross section from Rutherford scattering. The curves labeled "optical model" were calculated with waves distorted by the nuclear optical potential as well as the Coulomb field, and show marked changes. There is a considerable reduction in both elastic and inelastic cross sections at wide angles due to the reflection and absorption by the optical potential. The inelastic cross section is comparable to that induced by the purely nuclear interaction (26), as shown in Fig. 16. The Coulomb potential at the nuclear radius  $R_0$  is about 13 MeV, comparable to the alpha kinetic energies. At much lower energies the Coulomb repulsion effectively shields the nuclear interaction and the transition is predominantly electromagnetic. As the energy is raised, the nuclear contributions increase in importance. Of course, this transition from one mode of excitation to the other occurs at higher energies for heavier nuclei. In general, we may conclude that Coulomb excitation can be neglected, except for small scattering angles, provided the energy is well above the Coulomb barrier. However, as the energy approaches the barrier, Coulomb excitation becomes important and may be included in the above manner.

## VI. HIGHER ORDER EFFECTS

Two types of approximation have been made in our present treatment. First, we have solved the inelastic scattering problem to first order in the interaction, as-

suming that elastic scattering is predominant—the distorted-wave approximation. Higher order corrections here tell us how valid is this procedure. The second approximation is specific to our treatment in Section III of the nuclear collective model; in particular, the expansion in powers of the deformation  $\beta$  and the neglect of terms of order  $\beta^2$  and higher. The importance of these higher order terms reflects upon the significance of our interpretation in terms of this model.

### A. Strong Coupling

When the interaction strength increases, and the inelastic cross section becomes comparable to the elastic, the first-order distorted-wave Born approximation is inadequate. For example, virtual excitation of the excited states begins to affect the elastic scattering. An important aspect of this concerns conservation of flux; the number of scattered particles cannot exceed the number incident. (Equivalently the corresponding scattering matrix must be unitary; we return to this point in the following paper.)<sup>14</sup> However, in the first-order treatment, the inelastic cross section is proportional to the square of the interaction strength, so must be inadequate when the strength is large.

When the coupling is strong, we are obliged to solve for elastic and inelastic transitions simultaneously; formally the Schrödinger equation may be reduced to a set of coupled radial equations.<sup>21</sup> Such a calculation was carried out<sup>11</sup> for 43-MeV alphas on Ni, using a deformation of  $\beta=0.2$  (typical for this mass region), and compared with the distorted-wave calculation using the same optical potential. Only the coupling between the ground state and 1.45-MeV excited state was included. It was found that there is little difference for scattering angles in the forward hemisphere. At forward angles the distorted-wave method overestimates the inelastic cross section by about 10%; this discrepancy has increased to about 20% at 60°. The difference is larger at backward angles, the optical model and distorted waves overestimating both elastic and inelastic cross sections, although the oscillatory behavior of the angular distributions is similar in both cases.

In practice, these differences are partly taken into account by adjusting the optical potential parameters used in the distorted-wave calculation; this is done implicitly when the optical potential is adjusted to fit the observed elastic scattering. We conclude then that the distorted-wave method is quite accurate at this energy, especially for forward scattering angles. When the deformation becomes much larger than  $\beta=0.2$ , preliminary results indicate that the diffraction structure of the angular distribution is preserved, especially at forward angles, but the cross section does not increase like  $\beta^2$ . In such cases the distorted-wave method may

give a reasonable account of the angular distributions, while underestimating the deformation.

### B. The Nuclear Model

Use of the collective model is itself an approximation, albeit a reasonable one, as discussed in the introduction. However, we are here concerned with further approximations and uncertainties involved in its use. One uncertainty has already been illustrated by the two alternative ways, Eqs. (20) and (29), of defining the deformed potential well. Fortunately, these only lead to slight differences in the scattering.

Another uncertainty involves the use of the absorptive potential. This will also be nonspherical when the nucleus is deformed and could then contribute to the inelastic scattering. The calculations reported above have neglected this contribution. If the imaginary well has the same shape as the real, ( $r_0=r_0'$  and  $a=a'$  in Eq. (43)), the only effect is to increase the cross section by a factor  $1+(W/V)^2$ . For the case shown in Fig. 2 this is an increase of 8%, and so leads to deformations 4% smaller. If the imaginary potential has a shape different from the real well, its contribution to the inelastic amplitude must be computed with the correspondingly

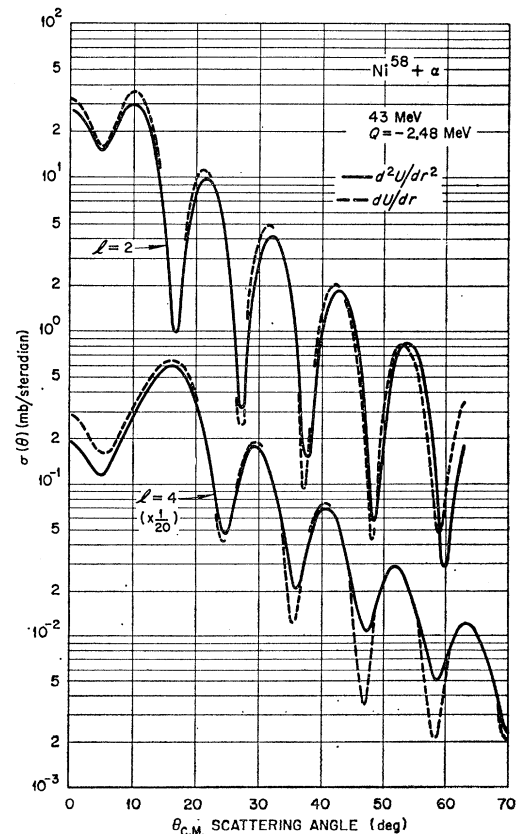


FIG. 18. Comparison of angular distributions induced by the first- and second-derivative interaction form factors of Eqs. (37) and (50), respectively, for 43-MeV alphas on Ni.

<sup>21</sup> S. Yoshida, Proc. Phys. Soc. (London) **A69**, 668 (1956); J. R. Lamarsh and H. Feshbach, Phys. Rev. **104**, 1633 (1956); D. M. Chase, L. Willets, and A. R. Edmonds, *ibid.* **110**, 1080 (1958).

different (and imaginary) form factor (namely using  $R_0' = r_0' A^{1/3}$  and  $a'$ ), and will interfere with the amplitude from the real well. The insensitivity of the shapes of the *cross sections* to variations in  $R_0$  and  $a$ , as shown in Fig. 14, suggests this interference effect may be small. This was checked explicitly in one case by adding the two amplitudes; the only effect was some filling of the minima in the inelastic angular distribution.

Next, we discuss the terms of order  $\beta^2$  in the expansion (23) of the interaction potential. These are associated with the second derivative of the optical potential, so for a Woods-Saxon potential they have a form factor

$$F(r) = (d^2/dx^2)(e^x + 1)^{-1}, \quad x = (r - R_0)/a. \quad (50)$$

In the vibrational mode, these terms are quadratic in the operators  $\alpha_{ka}$ , and cannot contribute to the excitation of a single phonon. They can excite two-phonon states, however; in particular, the quadrupole deformation in second order can give rise to  $l=4$  transitions. The excitation has been observed<sup>16,22</sup> of states in even nuclei known to be  $4^+$ , which are often regarded as members of the two-phonon triplet of states. The angular distributions were anomalous in the sense that they disobeyed the parity phase rule and oscillated "in phase" with the elastic angular distribution. Such transitions can be explained by the Fraunhofer diffraction model when expanded to second order in the deformation,<sup>23</sup> and it was believed initially that using the second-order

interaction in the distorted-wave method would also explain them. This belief was supported by the results of calculations using plane waves, in which it was also estimated that the two-step process (with intermediate excitation of the one-phonon  $2^+$  state) gave a negligible contribution.<sup>24</sup> However, Fig. 18 shows that the reduced cross sections predicted by form factor (50) are very close to those predicted by the first-order form factor, Eq. (37), with no change of phase of the oscillations in the angular distributions. This is opposite to the predictions when plane waves are used, and is due to the localization of contributions to the scattering from a region somewhat outside  $R_0$  which occurs when the optical-model distorted waves are used. In this region, as we see from Fig. 1, the two form factors are closely similar both in shape and magnitude. The discrepancy between these results and both experiment and the diffraction model are now known to be due to the two-step transitions which have an intensity comparable to the direct transitions considered here.<sup>11</sup> This again is in strong contrast to predictions of the plane-wave theory, and may be understood qualitatively from the structure of the second-order, distorted-wave Born approximation.<sup>25</sup>

#### ACKNOWLEDGMENTS

We are indebted to N. Austern for many valuable discussions in the course of this work, to L. W. Owen for assistance with the calculations, and to Joanne Rayburn for assistance with the programming.

<sup>22</sup> R. Beurtey, P. Catillon, R. Chaminade, M. Crut, H. Farragi, A. Papineau, J. Saudinos, and J. Thirion, *Compt. rend.* **252**, 1756 (1961).

<sup>23</sup> S. I. Drozdov, *Soviet Phys.—JETP* **11**, 362 (1960); J. S. Blair (private communication, 1961).

<sup>24</sup> R. H. Lemmer, A. de-Shalit, and N. S. Wall, *Phys. Rev.* **124**, 1155 (1961).

<sup>25</sup> N. Austern (to be published).